Available online at www.sciencedirect.com
ScienceDirect
Acta Materialia 59 (2011) 4525–4537
Acta MATERIALIA
www.elsevier.com/locate/actamat

Shear-band toughness of bulk metallic glasses

M.Q. Jiang, L.H. Dai *

State Key Laboratory of Nonlinear Mechanics, Institute of Mechanics, Chinese Academy of Sciences, Beijing 100190, People's Republic of China

Received 3 November 2010; received in revised form 29 March 2011; accepted 29 March 2011
Available online 29 April 2011

Abstract

Dynamic "forced" shear and quasi-static tensile tests were performed on a typical Vitreloy 1 bulk metallic glass (BMG). The nanoscale shear band is found to initiate in a local plastic region, then propagates with a well-defined front. A theoretical model that takes into account momentum, energy and free-volume balance is developed to quantitatively describe the dissipation system of shear-band propagation in the local plastic region. The analytical expressions for shear-localization time, shear-band thickness and critical energy dissipated within the band are obtained. Calculations demonstrate that the shear-band propagation process is dominated by the free-volume softening, rather than the thermal softening. The latter increases the band thickness slightly but decreases the corresponding critical dissipation energy somewhat. The concept of shear-band toughness is further introduced to measure the inherent resistance capability of materials to the propagation of shear bands in BMGs. These results assist in more comprehensively understanding the evolution mechanism of the shear bands, and in guiding alloy design to enhance the toughness of BMGs.

Keywords: Bulk metallic glass; Shear band; Free volume; Energy dissipation; Toughness

1. Introduction

Shear-banding instability continues to afflict bulk metallic glasses (BMGs) [1–3], although these materials have room-temperature (RT) strengths and elastic limits significantly in excess of those of polycrystals with comparable compositions [4–6]. The multiplication of shear bands can contribute considerably to global compressive [7–9] or bending ductility [7,10], but is almost helpless for improving tensile ductility. Therefore, it is still necessary to understand the nature of the shear-banding process in these glassy alloys. In this respect, areas of interest involve the geometrical configuration of shear bands, such as thickness [2,11,12], length and spacing [10,13–16], the structural change [17–19] and temperature rise [19–21] that occurs in shear bands, the propagating mode [19,22–26] and velocity of shear bands [27–29], and the deformation accommodated by shear bands, including plastic strain and its strain rate [30,31]. In fact, the critical plastic energy Γ_c dissipated in a shear band prior to catastrophic fracture is of central importance in the development of ductile BMGs. Once the energy release Γ overcomes the critical plastic energy Γ_c, the shear banding will mature as a runaway shear crack [32,33]. In this regard, a larger Γ_c indicates more significant toughness or ductility of BMGs. Γ_c therefore determines the shear-band susceptibility, which measures the intrinsic resistance of materials to propagation of shear bands. In our previous work [24,31], whether the shear band initiates easily or with difficulty can be characterized by the internal length and time scales for shear instability. Recent studies [32,33] have focused on the energy release Γ, and further experimentally determined the Γ_c. However, how to theoretically describe the inherent susceptibility Γ_c to shear-band propagation in BMGs has not been resolved yet. In the present work, we develop a concept of shear-band toughness, introduced by Grady [34,35], to characterize the shear-band susceptibility in BMGs, based on meticulous investigations of the propagating mode of mature shear bands in a typical Zr-based BMG. The underlying physics are discussed as well.

* Corresponding author. Tel.: +86 10 52843958; fax: +86 10 82543977.
E-mail addresses: mqjiang@imech.ac.cn (M.Q. Jiang), lhdai@lnm.imech.ac.cn (L.H. Dai).

1359-6454/$36.00 © 2011 Acta Materialia Inc. Published by Elsevier Ltd. All rights reserved.
doi:10.1016/j.actamat.2011.03.075

2. Experimental

Master alloy ingots with the nominal composition $Zr_{41.2}Ti_{13.8}Cu_{10}Ni_{12.5}Be_{22.5}$ (Vitreloy 1) were prepared by arc-melting the elements Zr, Ti, Cu, Ni and Be (with a purity of 99.9% or better) together in a Ti-gettered high-purity argon atmosphere. To ensure homogeneity, the ingots were re-melted several times and subsequently suction-drawn into copper molds to form rods ($\Phi 8 \times 80$ mm) and plates ($100 \times 20 \times 2$ mm). As shown in Fig. 1, the glassy nature of these rods and plates were checked by X-ray diffraction (XRD) in a Philips PW 1050 diffractometer using CuKα radiation. The XRD patterns showed only broad diffraction maxima and no peaks of crystalline phases were visible, indicating glassy structures.

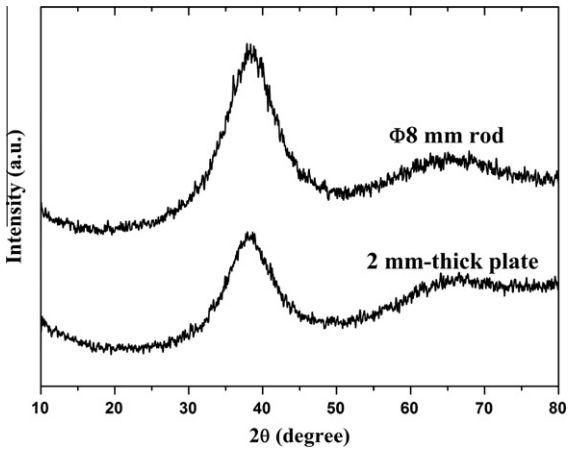

Fig. 1. XRD patterns of as-cast Vitreloy 1 BMG rod and plate.

Hat-shaped specimens have been used successfully to study the shear banding in various crystalline metals or alloys [36–39]. Here, we applied this configuration to BMG materials for the first time. The hat-shaped specimens (see Fig. 2a) were obtained by lathe machining the as-cast Vitreloy 1 rods using coolant. The dimensions of hat-shaped specimen were specially designed, as illustrated in Fig. 2b. By adjusting the height x of the top bar and controlling the striker velocity, different degrees of shear deformation with different strain rates could be achieved. Dynamic "forced" shear tests were performed with a split Hopkinson bar (Fig. 2c) following this procedure. First, the hat-shaped specimen was sandwiched between the incident and transmitted bars, as shown in the inset to Fig. 2c. The launched striker driven by high-pressure gas was impacted onto the free end of the incident bar. At the moment of impact, the elastic wave generated in the incident bar compresses the top bar, which is displaced into the bottom ring. This produces shear localization in the connection area between the bar and the ring, as marked by the red areas in Fig. 2b. Dogbone-shaped specimens with gauge sizes of $3 \times 2 \times 2$ mm were machined from the as-cast plates for tensile tests. Quasi-static tension tests

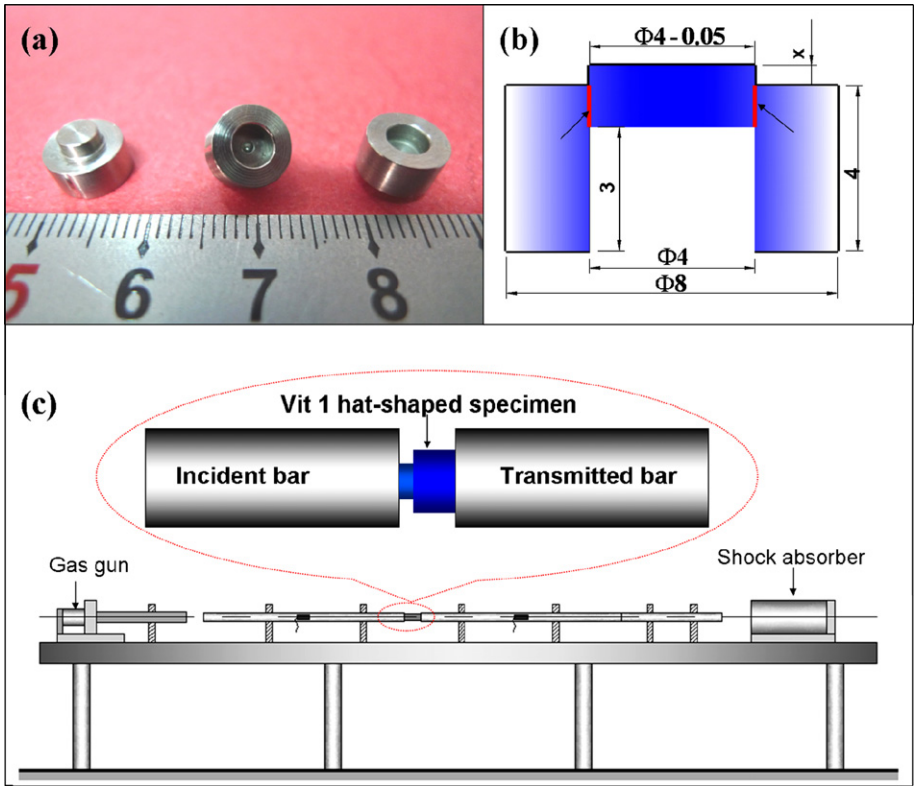

Fig. 2. (a) Hat-shaped specimens and (b) their geometrical configuration (dimensions in mm). (c) Schematic for a dynamic "forced" shear test of the hat-shaped specimen.

were conducted with an MTS-810 machine [40]. After testing, an FEI Sirion high-resolution scanning electron microscope with a spatial resolution of 1.5 nm and a Veeco DI MultiMode atomic force microscope (AFM) with spatial resolutions of 1 nm (horizontal) and 0.1 nm (vertical) were used to characterize the shear bands of all specimens.

3. Results

3.1. "Forced" shear test

The inset to Fig. 3a shows a deformed specimen with the initial height $x(\approx 0.5$ mm) of its top bar. Since the top bar is totally compressed into the bottom ring, the macroscopic shear displacement is about 0.5 mm. The width of the shear zone size normal to the shearing direction is prescribed to be about 0.05 mm. Thus, the shear strain rate can reach $\sim 2 \times 10^5\ s^{-1}$ at the present striker velocity ($\sim 11.5\ ms^{-1}$). In order to examine such a dynamic shear localization process, we first cut the specimen parallel to the shear direction, as illustrated in Fig. 3a. The cut section was polished using 0.5 μm diamond particles. Fig. 3b shows the left shear zone as marked by "L" in Fig. 3a. It can be seen that the crack with the well-defined tip does not penetrate through the shear zone. This implies that the local material has a high resistance to the present large shear deformation. Fig. 3c is a magnified scanning electron microscopy (SEM) picture corresponding to the area marked in Fig. 3b. The shear is along the vertical direction. As shown in Fig. 3c, the boundary line between the lighter region and the darker region clearly denotes a nanoscale shear band ahead of the crack tip. The presence of the lighter and dark regions is due to the angled irradiation of the electron beam. However, the right shear zone, marked "R" in Fig. 3a, displays a distinct feature. Under the same macroscopic shear displacement, the local material undergoes the full cracking that would be induced by a shear band, as shown in Fig. 3d. This observation indicates that, even for a given BMG, the resistance to shear deformation varies from one local material site to the next. This point is further confirmed in the following. The inset to Fig. 3e presents the AFM three-dimensional (3-D) landscape of the shear band in Fig. 3c, and clearly exhibits a well-defined tip nucleated at an inhomogeneous site. A more precise structure of the shear band is shown in Fig. 3e. Fig. 3f gives the surface profile across the shear band, i.e. the section "O" in Fig. 3e. One can clearly see that the shear band has a thickness of ~20 nm. Fig. 3g presents the surface profile along the shear band, i.e. the section "P" in Fig. 3e, showing a relatively smooth morphology with a height fluctuation of less than 10 nm.

Furthermore, a specimen (see the inset to Fig. 4a) with the same macroscopic deformation as that in Fig. 3a was cut perpendicular to the shear direction, as indicated in Fig. 4a. The material in the shear zone (circled by the red line in Fig. 4a) should be subject to identical shear deformation. However, it is surprising to note that shear bands and cracks exist alternately along the circumferential direction in the shear zone, as shown in the inset to Fig. 4b. Such alternative existence eliminates the effect of asymmetrical loading. This is the reason why asymmetrical failure can be observed in the shear zone on an arbitrary vertical section plane (e.g. Fig. 3). A close-up view of the region marked in the inset to Fig. 4b is displayed in Fig. 4b. Clearly, the crack is led by a shear band. In order to obtain the detailed information about shear banding, we scanned this area (marked in Fig. 4b) by using AFM again. A crack was probed, and its 3- and 2-D landscapes are shown in Fig. 4c and d, respectively. In front of the crack, an obvious shear band can also be observed, as shown in Fig. 4e. Its 2-D image is presented in Fig. 4f.

3.2. Uniaxial tension test

A fractured tensile specimen is presented in Fig. 5a, showing a shear-dominant failure mode with a main shear-fracture plane [40]. Fig. 5b shows the top view of the fracture plane. The fracture surface is relatively smooth, and micrometer-scale river-like vein patterns are visible. Fig. 5c is a high-magnification micrograph of the area circled in Fig. 5b, displaying a side view of a stopped shear-failure plane. It can be seen from this figure that the evolution of a shear band can lead to a crack formation and failure. As indicated in Fig. 5d, a melted droplet on the main shear plane is cut into two parts by the shear band in front of the crack. The displacement between the two parts of the droplet along the shear direction is measured to be about 30 nm. The crack ensues immediately after the shear band (see Fig. 5c). This implies that the necessary displacement of a shear band to develop into a crack is also tens of nanometers even in the quasi-static case. Fig. 5d provides solid support for the shear strain (~100%) of a shear band, which is consistent with the estimated strain, i.e. 1–10, in a bent sample [41]. It is noted that the crack on the neck of the shear band has an open displacement of only tens to hundreds of nanometers, as shown in Fig. 5e. At the final stage of the crack, a significant melted belt can be observed, as marked in Fig. 5c, which indicates that the temperature rise during the final failure event may exceed the melting temperature of the alloy.

3.3. Information extracted from experiments

In order to gain a fundamental knowledge of shear-band propagation in BMGs, it is important to highlight several unique shear-banding behaviors:

(1) Shear banding occurs in a progressive fashion, namely, it initiates from a localized front and then propagates. This shear-band propagation mode has been widely observed in the literature [1–3,6,13,21–23,25,26,42,43] and in our previous study [24]. If the crack could be arrested, the propagating shear band

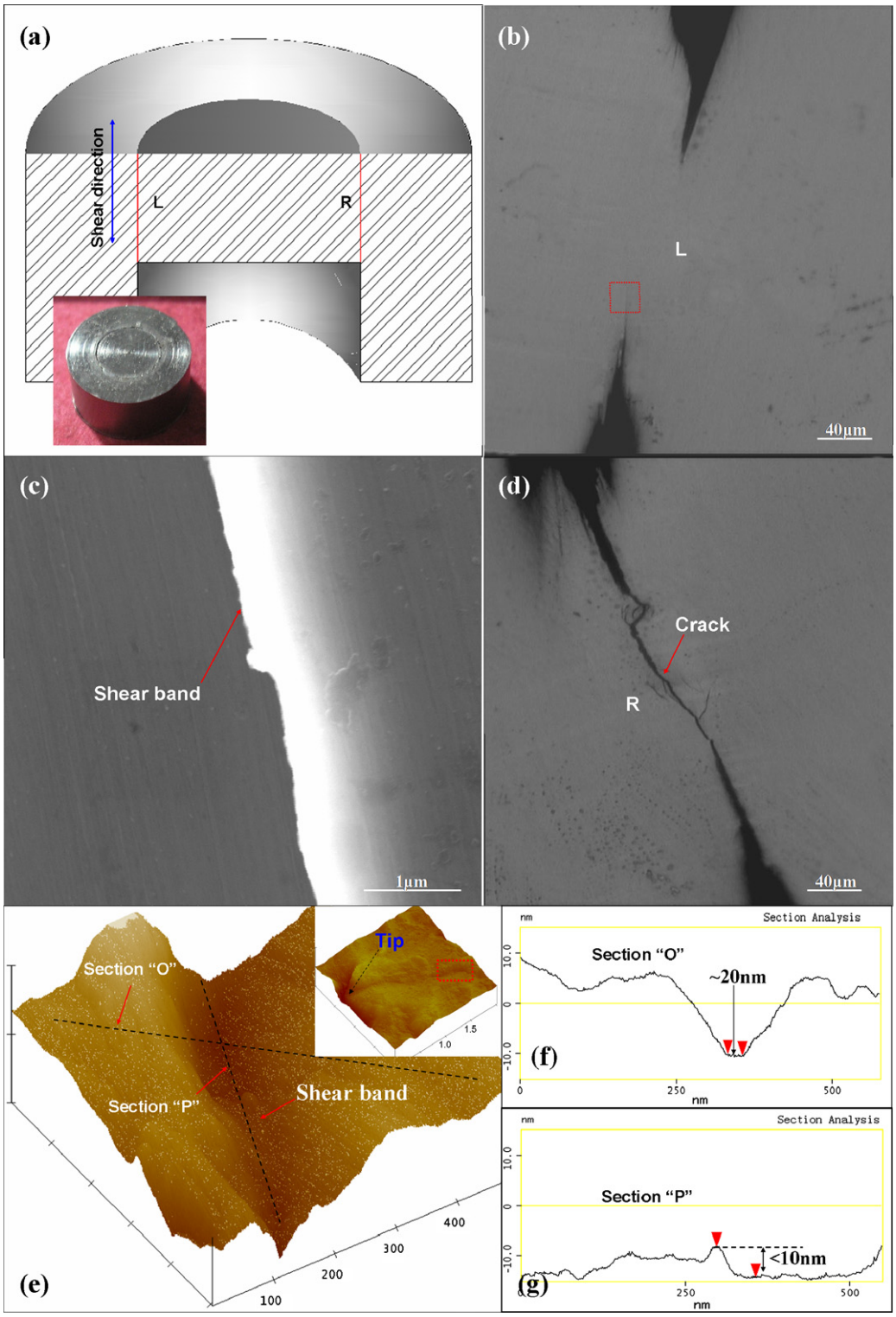

Fig. 3. (a) Longitudinal section of a deformed hat-shaped specimen (Inset). (b) SEM image showing the area marked "L" in (a). (c) Details corresponding to the area marked in (b). (d) Right shear zone marked "R" in (a). (e–g) AFM results of the shear band in (c).

would finally penetrate the entire sample to reach the opposite surface. In this case, the shear band would operate in a simultaneous fashion; this is expected to occur in some ductile systems. Recently, Cao et al. [19] captured the transition of shear-banding mode from the progressive at small sample strains to simultaneous fashion at very larger strains, using molecular dynamics simulations.

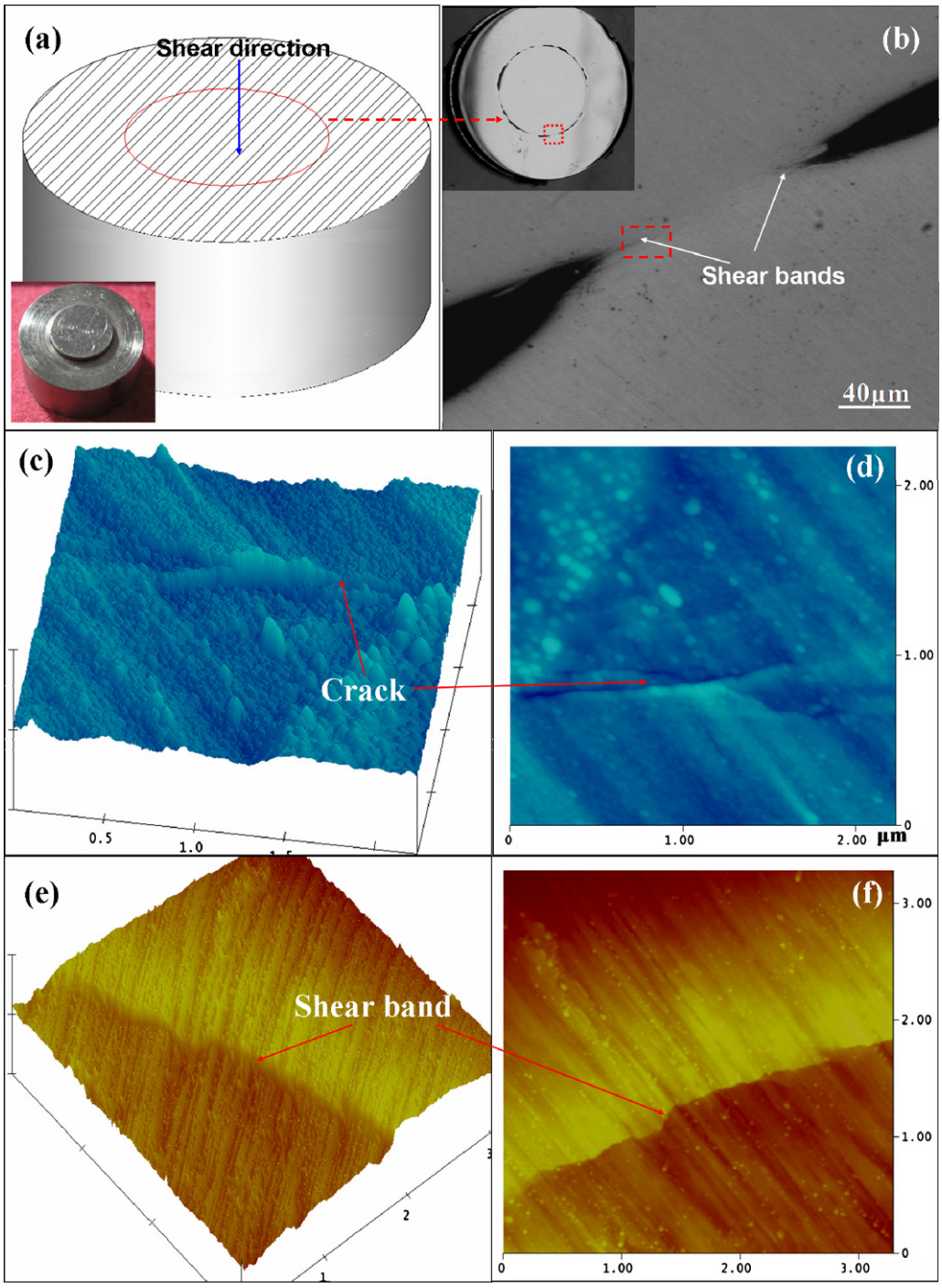

Fig. 4. (a) Horizontal section of a deformed hat-shaped specimen (Inset). (b) Shear zone marked in (a) at different magnifications. (c–f) AFM results of the area marked in (b), showing the 3- and 2-D cracks and shear bands.

(2) For the present dynamic shear or quasi-static tension of Vitreloy 1 BMG, the shear band is very susceptible to developing into a shear crack with a shear displacement increase in only tens of nanometers. Based on the observation of polishing scratches, Yang et al. [21] measured shear displacements ranging from tens to hundreds of nanometers from the tip to the end of a shear band in a Zr-based BMG under quasi-static tension. These measured values are close to the shear offset at the surface of samples that must be due solely to a shear-banding process. Hampel and Neuhäuser [44] captured images of the formation of shear offsets on the surface of a metallic glass ribbon deformed in bending through the use of an optoelectronic technique. They found that the shear offsets ranged from 30 to 120 nm. A similar shear offset value (~100 nm) was also observed by Chen et al. [45] in Al-based ribbons in bending. Remarkably, a

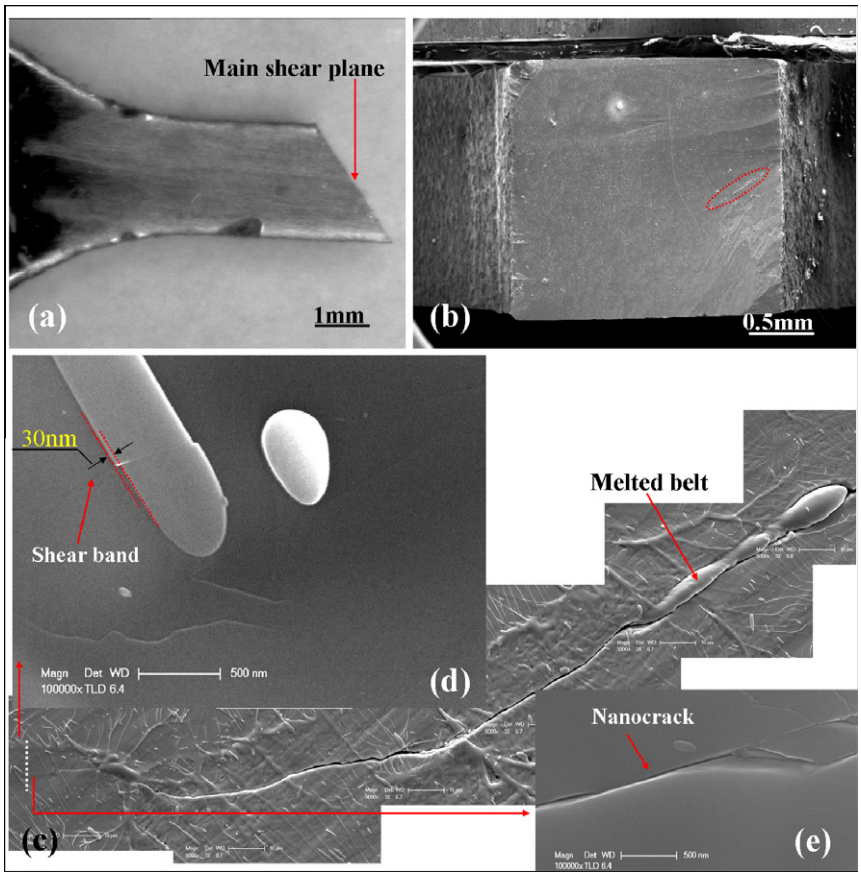

Fig. 5. Fracture features of Vitreloy 1 BMG under quasi-static tension. (a) Side view of the fractured specimen. (b) SEM image showing a top view of the main fracture surface. (d–f) Details corresponding to the area circled in (b), clearly showing a nanoscale shear band followed by a crack.

smaller shear displacement of the order of a few nanometers is expected in nanoindentation [46]. Note that shear displacements of a micrometer up to tens of micrometers were observed in quasi-static compressive tests [32,43,47], although the cracking unavoidably interferes. In order to encompass the above scenarios, the critical shear displacement of a shear band evolving into the crack is reasonably estimated to lie in range 100 nm to 10 μm.

(3) The shear band has a characteristic thickness of ~10 nm, suggesting its structural origin [11,12,20]. More specifically, the shear-banding instability in BMGs is dominated by local free-volume softening [12,30,48]. In addition, the heat-affected zone (HAZ) around the shear band observed by Yang et al. [42] and Guo et al. [43] as well as the melted belt at the final fracture surface (Fig. 5) imply that thermal softening could also play a role in shear band formation in BMGs [12,20,21,31,49].

(4) The evolution of a shear band into a crack is an extremely localized process within a BMG. In crystalline alloys, the shear banding or inhomogeneous plastic instability usually occurs after the entire sample experiences plastic deformation. However, the shear banding in BMGs initiates at some local regions where the viscosity or the resistance of the material to deformation is greatly reduced. Outside of these weak regions, the materials may still deform elastically [50,51].

These features pose a big challenge to quantitatively characterize the shear-band propagation in BMGs. This concern is considered further in the next section.

4. Shear-band toughness

4.1. Local evolution model for shear band

Unlike crystalline alloys, BMG specimens do not undergo full-field global plastic deformation when subjected to an external loading at RT. Instead, some local regions preferentially yield via the cascade of a number of individual atomic jumps around free-volume sites [52] or shear transformation zones [50,51], forming local plastic regions, as illustrated in Fig. 6. The shear bands then nucleate simultaneously or successively in these local plastic regions. Finally, one of the nucleated shear bands will dominate and cause a catastrophic fracture of the material.

The nucleation of a shear band was treated in our previous studies [2,24,31]. Here, we concentrate on the process

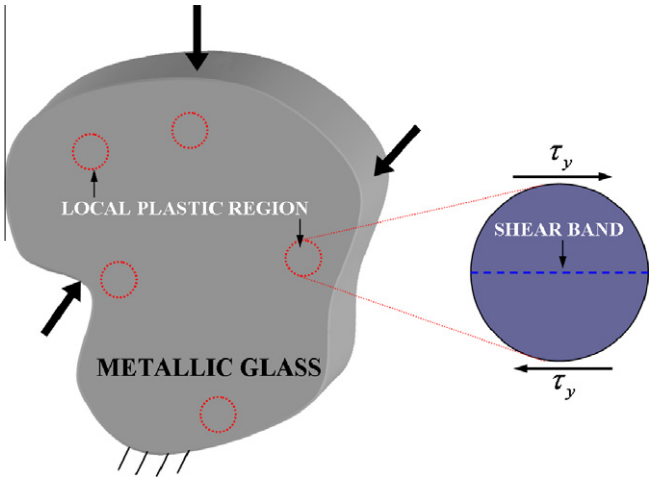

Fig. 6. Schematic diagram of shear band initiating in local plastic regions in a BMG subjected to external loading.

of shear-band evolution/propagation at the stage of growth in a local plastic region until it matures. It is well known that the shear-banding process is a dissipation system [2,10,15,16,31–33,37,53]. In addition to conventional thermal/energy and momentum/viscous dissipation, the free-volume dissipation should be involved here due to the unique atomic structure of BMGs. Three types of dissipation effects can be traced during the in situ or post-shear-banding process. For example, Lewandowski and Greer [20] have experimentally shown a significant temperature rise within the shear bands using tin-coated specimens, although such a thermal phenomenon is a secondary effect [11,19,31]. Moreover, the strain rates or time scales of loading often affect the spatiotemporal characteristics of shear bands [15,25,54]. In particular, a density fluctuation [17,55] and thus a viscosity drop [27,31,47] usually accompanies the shear-band evolution, implying the loss of short-to-medium-range order [19] or equivalently the coalescence of free volume [18,31] within the band.

Without losing the generality, the domain of interest only includes the half-space of local plastic region where a Lagrangian coordinate system (x, y) is attached. The coordinates x and y are normal and parallel to the direction of shear flow, respectively. In order to highlight the essential physics, we assume that the shear band initiates along the slip plane $x = 0$ at time $t = 0$, as shown in Fig. 7a. The shear band has a certain thickness a of the order of ~10 nm [11,12], which should be much smaller than the size l (usually ranging from millimeters to micrometers [15]) of the considered domain. The plane $x = 0$ corresponds to the center of the shear band. In order to render the theoretical derivation tractable, we adopt here the assumption of the constant shear-band thickness following Grady [34,35,56]. Hence, details of the shear band can be collapsed to a boundary displacement condition at $x = 0$. At initial time $t = 0$, the stress field (Fig. 7a) is

$$\tau(x \geqslant 0) = \tau_y \tag{1}$$

where τ_y is the flow stress of the material. This means that a homogenous shear flow is achieved in the local plastic region. The velocity field is given by

$$v(x) = \dot{\gamma}_l x \tag{2}$$

where $\dot{\gamma}_l$ is the average shear strain rates in the local plastic region.

Three modes of dissipation, as discussed above, occur within the propagating shear band. These several dissipation mechanisms lead to shear stress relaxation within the shear band as deformation evolves. This stress relaxation is related to the shear displacement ψ at boundary $x = 0$ obeying a softening law. When the shear stress $\tau(\psi)$ at the shear band vanishes (or the shear displacement reaches a critical ψ_c), the shear band is regarded as being fully mature, and a finite amount of energy is expended. On the other hand, the dissipations lead to free-volume, thermal and momentum diffusion out of the shear band and into the neighboring medium; thus stress release also occurs in the undisturbed medium.

We previously revealed that the free-volume diffusion determines the shear band thickness itself [12]; in the following, we will further verify this point. The momentum diffusion results in a rigid–plastic interface at the position $x = \zeta_1$, where ζ_1 is the distance from the shear band center to the boundary of the shear relaxed region (or rigid region), as shown in Fig. 7b. In the current analysis, the material is assumed to be rigid–ideal plastic for simplicity. The thermal diffusion produces a HAZ ($0 < x < \zeta_2$) adjacent to the shear band. During the propagation of the shear band, the two interfaces ($x = \zeta_1$ and $x = \zeta_2$) move away from the band. Since the momentum diffusion is much faster than the thermal diffusion, $\zeta_1 \gg \zeta_2$ and thus $v_1 = \dot{\gamma}_l \zeta_1 \gg v_2 = \dot{\gamma}_l \zeta_2$. The velocity of the rigid region is therefore controlled by the momentum diffusion rather than the thermal diffusion. Thus, the velocity field at later times, $t > 0$, is given by

$$v_1(x,t) = \begin{cases} \dot{\gamma}_l \zeta_1(t) & (0 \leqslant x \leqslant \zeta_1(t)) \\ \dot{\gamma}_l x & (\zeta_1(t) \leqslant x < l) \end{cases} \tag{3}$$

The momentum of the semi-local plastic region per unit area of the y plane corresponding to the velocity filed in Eq. (3) can be calculated as:

$$p_y = \int_0^{\zeta_1(t)} \rho \dot{\gamma}_l \zeta(t) \mathrm{d}x + \int_{\zeta_1(t)}^{l} \rho \dot{\gamma}_l x \mathrm{d}x \tag{4}$$

The motion of the adjacent rigid region is obtained by equating the time derivative of momentum in Eq. (4) to the misbalance of the shear stresses on its upper and lower boundaries, that is

$$\frac{\mathrm{d}p_y}{\mathrm{d}t} = \tau_y - \tau \tag{5}$$

Generally, τ is considered as a function of the boundary displacement ψ or shear band displacement, the time rate $\dot{\psi}$ of such displacement and some internal state variables $I_i (i = 1, 2, \ldots)$, and is given by

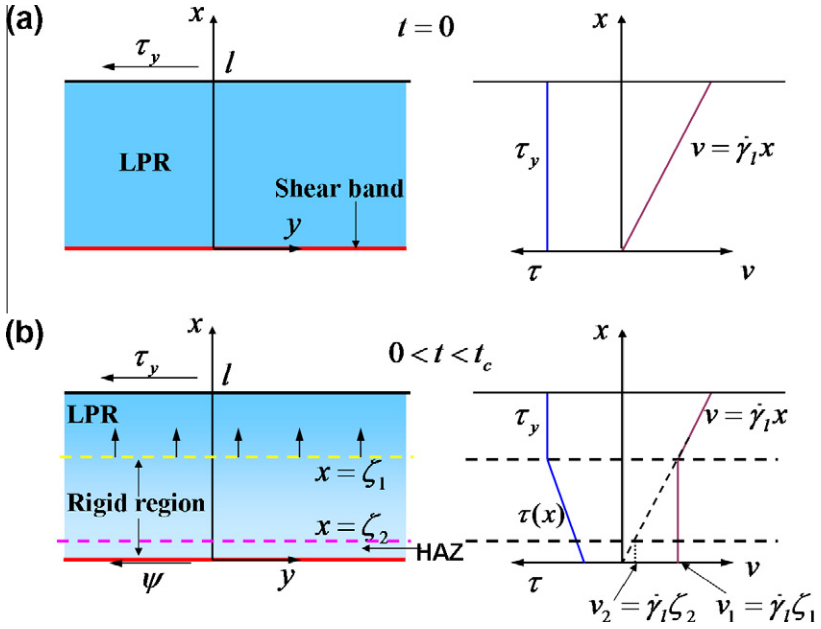

Fig. 7. Local evolution model for shear bands in BMGs. (a) Initial material field (left) and corresponding stress and velocity fields. (b) Material response (left) and corresponding stress and velocity fields during shear-band evolution.

$$\tau = \tau(\psi, \dot{\psi}, I_i) \tag{6}$$

Furthermore, it is noted that the rigid region $0 < x < \zeta_1$ moves at a constant velocity of

$$v_1(0) = v_1(\zeta_1) = \dot{\gamma}_l \zeta_1 \tag{7}$$

This compatibility condition requires that the boundary displacement at $x = 0$ satisfies

$$\frac{d\psi}{dt} = \dot{\gamma}_l \zeta_1 \tag{8}$$

If a specific form of the softening law (6) is determined, Eqs. (5), (6), and (8) can be solved numerically for a full solution for shear-band evolution of BMGs. However, a full solution of this system is not pursued here. In the present study, we undertake an analytical calculation to provide an approximate solution, focusing specifically on the critical energy dissipation during the shear-band propagation.

4.2. The Grady–Kipp solution

We first look back to the Grady–Kipp solution [34,35,56] in order to establish some basic and important relationships. Grady [34] applied the Mott solution [57] of dynamic fracture growth to an adiabatic shear-localization problem, assuming a linear relationship between stress release and boundary displacement in Eq. (6):

$$\tau = \tau_y \left(1 - \frac{\psi}{\psi_c}\right) (0 \leqslant \psi \leqslant \psi_c) \tag{9}$$

This particular form for stress relaxation with boundary displacement (or equivalently shear band growth) can lead to explicit analytic solutions. Substitution of Eq. (9) into Eq. (5) results in an ordinary differential equation:

$$\rho \dot{\gamma}_l \zeta_1 \frac{d\zeta_1}{dt} = \frac{\tau_y}{\psi_c} \psi \tag{10}$$

Then

$$\ddot{\zeta}_1 + \frac{1}{\zeta_1} (\dot{\zeta}_1)^2 = \frac{\tau_y}{\rho \psi_c} \tag{11}$$

Combining Eqs. (8) and (11) with their initial conditions, $\psi(0) = \xi(0) = 0$, leads to a solution for the rigid–plastic interface,

$$\zeta_1 = \frac{\tau_y}{6\rho\psi_c} t^2 \tag{12}$$

and boundary displacement,

$$\psi = \frac{\tau_y \dot{\gamma}_l}{18\rho\psi_c} t^3 \tag{13}$$

When $\psi = \psi_c$, a critical time for shear-band evolution is obtained,

$$t_c = \left(\frac{18\rho\psi_c^2}{\tau_y \dot{\gamma}_l}\right)^{1/3} \tag{14}$$

This relationship indicates that the duration for shear-band evolution depends on the density and flow stress of the material, the critical displacement accommodated in a shear band and the local strain rate in the vicinity of a shear band.

If we do not consider the softening nature of the linear stress–displacement relationship (9) for a while, Eq. (14) allows us to estimate the critical time for shear band to fully mature in BMGs. For the present Vitreloy 1 BMG [30], $\rho = 6125\ \mathrm{kg\ m^{-3}}$ and $\tau_y \sim 1$ GPa. Following Zhang et al. [15], we choose the local strain rates $\dot{\gamma}_l$ varying from 10^3 to $10^9\ \mathrm{s^{-1}}$ that are expected to encompass the

macroscopic loading rates from the quasi-static to dynamic range. In fact, in our previous analysis [31], we found that the $\dot{\gamma}_l$ can reach $\sim 10^3\ s^{-1}$, even at a macroscopic loading rate of $10^{-2}\ s^{-1}$. Fig. 8 shows the variations of the critical time in Eq. (14) with the local strain rate at different critical displacements. It can be seen from this plot that the critical time for the shear-band evolution into a crack increases with decreasing $\dot{\gamma}_l$ and increasing ψ_c. The predicted value of critical time t_c ranges from a few nanoseconds to a few microseconds. For very high strain rates, the shear band hardly propagates because $t_c \to 0$. This result explains why even state-of-the-art infrared and optical techniques with a high temporal resolution (from ms to μs) are not able to observe the complete shear-banding process [21,22,25,58,59]. The hat-shaped specimen technique could be an effective method to capture the shear-band propagation via frozen deformation [24,36–39]. It is also noted that the time for shear-band propagation is much smaller than the time scale for shear-band nucleation [31]. This implies that, in a monolithic BMG, the shear band initiates with difficulty, but propagates very easily. Once the shear band starts to propagate, it is very hard to stop it. Thus, it is expected that controlling the initiation of shear bands in favor of their multiplication or even homogeneous deformation is a more valid ductility enhancement methodology [7–9].

4.3. Shear-band dissipation energy and toughness

More and more works [12,15,16,18–21,31,47,49,59] have indicated that the shear-banding formation in BMGs is a coupled thermomechanical process, dominated by local free-volume softening and assisted by thermal softening. In order to capture such a coupling nature, we replace the shear stress softening relation in Eq. (9) with the form:

$$\tau = \tau_y(1 - \alpha \cdot \upsilon)(1 - \beta \cdot \theta) \tag{15}$$

where α is a free-volume softening coefficient, $\upsilon = \xi - \xi_0$ is the increase in free-volume concentration with initial value ξ_0, β is a thermal softening coefficient and $\theta = T - T_0$ is the temperature rise from an initial temperature T_0. Although the elementary constitutive relation in Eq. (15) is very simple, it highlights the softening properties of the shear band, i.e. the free-volume softening, the thermal softening and their interaction. In order to obtain an analytical solution, we neglect the cross-term that is small compared to the individual terms due to either the free-volume softening or the thermal softening. Therefore we have,

$$\tau = \tau_y(1 - \alpha \cdot \upsilon - \beta \cdot \theta) \tag{16}$$

Through Eqs. (9), (13), and (16), the time dependence of the increase in free-volume concentration of the shear-band can be determined from the mechanical solution, given by

$$\upsilon = \frac{\tau_y \dot{\gamma}_l}{18\alpha\rho\psi_c^2} t^3 - \frac{\beta}{\alpha}\theta \tag{17}$$

This relation indicates that, at the later stage of shear banding, the temperature rise decreases the increase in free-volume concentration, which is consistent with the previous numerical results [31,49]. However, it has been found that, during the process of the nucleation of shear band, the increase in temperature slightly speeds up the free-volume creation [31]. At $t = t_c$, substituting Eq. (14) into Eq. (17) yields

$$\upsilon_c = \frac{1 - \beta\theta_c}{\alpha} \tag{18}$$

where υ_c and θ_c are the critical values of free-volume concentration and temperature increase, respectively.

The free-volume evolution in the shear band can be expressed as the following equation [2,31,48]:

$$\frac{\partial \xi}{\partial t} = D\frac{\partial^2 \xi}{\partial x^2} + G^{\xi} \tag{19}$$

where D is the diffusion coefficient of free-volume concentration and G^{ξ} is the net generation rate of free-volume [52]. Defining $D_a = D/(a^2/2)$ and further integrating its weaker format of Eq. (19) over the critical time t_c, we get

$$\frac{1 - \beta\theta_c}{\alpha} = \int_0^{t_c} G^{\xi} \mathrm{d}t - \frac{D_a}{4} t_c \frac{1 - \beta\theta_c}{\alpha} \tag{20}$$

In addition, the energy balance requires that [53,54]

$$\theta_c = \frac{1}{2c_a}\tau_y\psi_c - \frac{\chi_a}{4} t_c\theta_c \tag{21}$$

where $c_a = \rho c a/2$ with specific heat c, and $\chi_a = \chi/(a^2/2)$, with χ being the thermal diffusivity. It is noted that the factor 1/2 in Eqs. (20) and (21) is an attempt to achieve a better average over t_c. Furthermore, the net generation rate of free volume G^{ξ} is assumed to be related to the shear strain rate $\dot{\gamma}_b$ in the shear band with [12,60–62]

$$G^{\xi} \approx R\dot{\gamma}_b \tag{22}$$

where the parameter R describes the molar volume (normalized by the effective hard-sphere size of the atom) produced by a unit plastic shear strain [60], denoting the local dilatation ability.

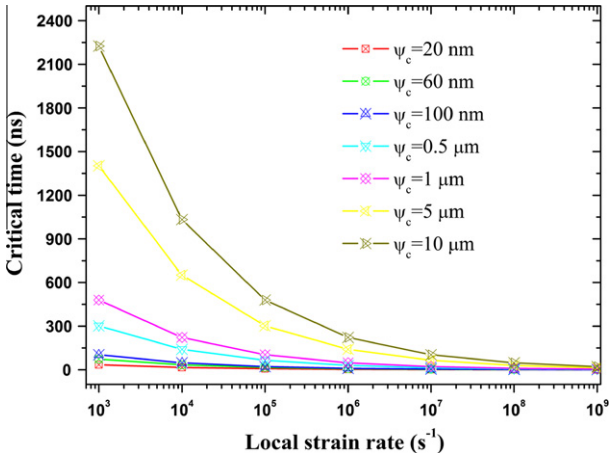

Fig. 8. The critical shear time vs. the local strain rate with different critical shear displacements.

We now introduce the critical energy Γ_c dissipated within the shear band as deformation proceeds to a critical displacement ψ_c. Consistent with concepts of fracture mechanics [63], Γ_c is the energy dissipated per unit area within one-half of the shear band, identified as

$$\Gamma_c = \frac{1}{2}\tau_y\psi_c \tag{23}$$

Combining Eqs. (14) and (20)–(23) results in an implicit expression of the critical dissipation energy Γ_c:

$$\left[1 - \frac{2\beta}{\rho c a}\frac{\Gamma_c}{1+\frac{\chi}{\tau_y a^2}\left(\frac{9\rho}{\dot\gamma_l}\Gamma_c^2\right)^{1/3}}\right]\left[1+\frac{D}{\tau_y a^2}\left(\frac{9\rho}{\dot\gamma_l}\Gamma_c^2\right)^{1/3}\right] = \frac{2\alpha R}{\tau_y a}\Gamma_c \tag{24}$$

If we do not consider the thermal softening effect, i.e. let $\beta = 0$, Eq. (24) then simplifies to

$$\Gamma_c^2 = \frac{\tau_y^3 a^6 \dot\gamma_l}{9\rho D^3}\left(\frac{2\alpha R}{\tau_y a}\Gamma_c - 1\right)^3 \tag{25}$$

It was found that the shear-band propagation always seeks a maximum growth rate, which is equivalent to a minimum energy dissipation in the shear-band relaxation process [34,35]. Thus, according to the minimum energy principle

$$\left.\frac{\partial\Gamma_c}{\partial a}\right|_{a_0} = 0 \tag{26}$$

we obtain an optimum shear-band thickness in the case of solely free-volume softening:

$$a_0 = \left(\frac{9\rho D^3}{\dot\gamma_l\tau_y\alpha^2R^2}\right)^{1/4} \tag{27}$$

Further, the dissipation energy corresponding to the thickness a_0 is also obtained as

$$\Gamma_{c0} = \frac{\tau_y}{\alpha R}a_0 \tag{28}$$

Following Grady [34,35], the concept of shear-band toughness is naturally introduced as follows:

$$K_{s0} = \sqrt{2\mu\Gamma_{c0}} \tag{29}$$

where the shear modulus $\mu = 35.3$ GPa for the Vitreloy 1 BMG [31]. The shear-band toughness (29) is analogous to the concept of fracture toughness and measures the internal resistance of BMG materials to the propagation of a shear band. The factor 2 is used in Eq. (29) because the above considerations apply to only one-half of the shear band. In terms of a_0 and Γ_{c0}, and further considering $\chi \gg D$, Eq. (24) can be nondimensionlized as

$$\left[1-\Omega(\Gamma_c/\Gamma_{c0})^{1/3}(a/a_0)\right]\left[1+\frac{(\Gamma_c/\Gamma_{c0})^{2/3}}{(a/a_0)^2}\right] = 2\frac{(\Gamma_c/\Gamma_{c0})}{(a/a_0)} \tag{30}$$

with a dimensionless thermal-effect coefficient,

$$\Omega = \left(\frac{2}{\alpha R}\right)\left(\frac{B}{\mathrm{Le}}\right) \tag{31}$$

where $B = \tau_y/(\rho c/\beta)$ accounts for the degree of thermal softening, and the Lewis number $Le = \chi/D$ measures the competition between thermal diffusivity and free-volume diffusivity. Eq. (30) provides the implicit expression for energy dissipation in a coupled free-volume–thermal-softening shear band with a thickness of a. In this case, the shear-band toughness can be defined as

$$K_s = \sqrt{\Gamma_c/\Gamma_{c0}}K_{s0} \tag{32}$$

To apply the analytical expressions for shear-band dissipation energy and toughness, material parameters, appropriate to the current dynamic shear deformation in Vitreloy 1, must be established. Based on the above results, Γ_c in Eq. (23) should be of the order of $\sim 10^2$–10^4 J m^{-2}, which usually compares with the order of Γ_{c0} in Eq. (28). As a result, we can obtain an order of the product of α and R of $\sim 10^{-1}$–10^{-3} because of the shear-band thickness a_0 of $\sim$10 nm [11,12]. Furthermore, the order of D can be estimated to be 10^{-10}–10^{-8} m^2 s^{-1} according to Eq. (27) and considering $\dot\gamma_l \sim 10^3 - 10^9$ s^{-1} [15]. For alloys, the thermal softening coefficient usually ranges from 10^{-4} to 10^{-3} K^{-1} [34,56]. From these, a value range of $\Omega \sim 10^{-1}$–10^{-4} is obtained based on the relation (31).

The functional dependence of the critical dissipation energy on the shear-band thickness under different thermal-effect coefficients, determined by Eq. (30), is shown in Fig. 9. For comparison, we calculate the case without the thermal effect, i.e. $\Omega = 0$, corresponding to the bold green line. From this graph, it is readily seen that all these curves have two branches, left and right, both of which intersect at a local minimum. The physical mechanism responsible for the observed behavior is reasonably clear. For thinner bands (moving to the left branch) the enhanced free-volume diffusion restrains the rate of free-volume softening and leads to excessive dissipation [31,53]. Thicker bands (moving to the right branch) are effectively free of free-volume diffusion. However, the accelerated diffusion of momentum (inertia) into the shear-band vicinity again limits the rate of free-volume softening and also incurs additional dissipation. The shear-band thicknesses near the local minimum properly balance the free-volume and momentum diffusion, providing the minimum possible shear-band dissipation. During the competition between the free-volume and momentum diffusion, the thermal softening, including its diffusion, plays a secondary role. As shown in Fig. 10, with the thermal-effect coefficient Ω increasing from 10^{-4} to 10^{-1}, the optimum shear-band thickness increases slightly from a_0 to about 1.2 a_0; the corresponding optimum shear-band dissipation energy decreases somewhat from Γ_{c0} to 0.75 Γ_{c0}. This result clearly indicates that the thermal effect promotes the shear-band propagation since it decreases the critical

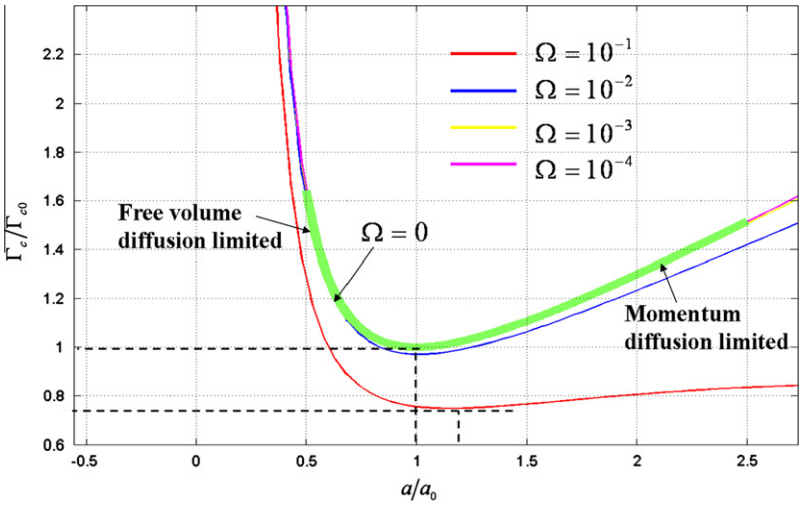

Fig. 9. Plot of the critical energy dissipated in the shear band as a function of the shear-band thickness. All curves are provided by Eq. (30) in the text with different thermal-effect coefficients and are nondimensionalized by the optimum shear-band thickness a_0 (27) and the corresponding dissipation energy Γ_{c0} (28) for the sole free-volume softening case.

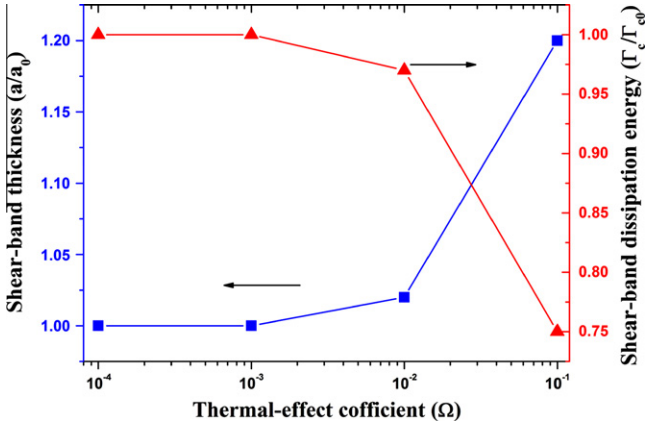

Fig. 10. Influence of the thermal effect on the optimum shear-band thickness and corresponding critical dissipation energy within the band.

energy barrier, thus preventing the shear band from cracking. In particular, the insensitivity of the shear-band thickness to thermal softening indicates that the shear-band propagation in BMGs is governed by the free-volume softening. This result is consistent with our previous analysis [12].

Base on the calculated shear-band dissipation energy in Fig. 10 and using Eqs. (28), (29), and (32) , we obtain for the present Vitreloy 1 BMG a shear-band toughness of $K_s \sim (2.66 - 26.58)$ MPa$\sqrt{\text{m}}$, if considering the critical displacement ψ_c varies from 100 nm to 10 μm. This calculated value range of K_s is expected to be smaller than the mode II fracture toughness ($K_{\text{IIC}} = 75$ MPa$\sqrt{\text{m}}$) of this material measured by Flores and Dauskardt [64]. Such a difference is physically reasonable, arising from the extreme localization of plastic flow ahead of the crack tip. In crystalline alloys with relatively global plasticity, the predicted adiabatic shear band toughness is close to the extensional fracture toughness [34]. In addition, attention should be paid to the following aspects. (i) In the real measurement, normal or mean stresses play a significant role in the deformation process at the crack tip, which also contributes to fracture toughness [64]. Recently, Zhang et al. [15,47] undertook a theoretical investigation of the effect of normal stress on shear-band propagation and showed that the normal stress results in more energy being dissipated within the shear band, indicative of a larger temperature rise. However, a pure shear deformation is considered in our present model. (ii) The current model considers only one shear band, whereas the multiplication, branching and intersection of shear bands must occur in experiments [65]. These shear bands will consume more energy and thus increase fracture toughness remarkably. (iii) It should be borne in mind that the shear of randomly close-packed atoms can cause dilatation [17,66,67] and vice versa [68]. Thus, fracture energy dissipates not only in the shear-banding mode but also via new surface formation [40], although the former plays a dominant role in most cases. Extension of the shear-band toughness to the fracture toughness is beyond the scope of this paper.

Nevertheless, it can be argued that the shear-band toughness would contribute to the fracture toughness, because the activation of shear bands ahead of the crack tip expends more energy [65,69,70]. Our results therefore provide some important clues for enhancing the fracture toughness that is a desirable property for BMGs. Increasing the shear modulus μ (see Eq. (29)) will increase the fracture toughness, which is consistent with the experimental data collected by Lewandowski et al. [71]. Furthermore, it is found from Eqs. (27)–(29) that the fracture toughness will increase with increasing flow stress τ_y, density ρ and free-volume diffusibility D, but decreasing local strain rate $\dot{\gamma}_l$, free-volume softening coefficient α and local dilatation R. Recent experiments have actually shown that dilatation or tension usually results in the brittle fracture (or

equivalently low fracture toughness) of BMGs [40,72,73]. Finally, the temperature rise and accompanying thermal softening are detrimental to the shear-band toughness, as is illustrated in Fig. 9.

5. Conclusions

The shear band propagation process in BMG is studied through both experiments and approximate analytic methods. The shear band is found to propagate in a progressive fashion with a well-defined tip. Theoretical expressions for shear-band growth time, thickness and dissipation energy are derived by viewing the shear band as a dissipation source. The optimum shear band thickness and corresponding critical dissipation energy are revealed to be determined by the balance between the momentum and free-volume diffusion, wherein the thermal effect plays a secondary role. Based on the critical energy dissipated within the shear band, the shear-band toughness is proposed to quantitatively measure the susceptibility of the shear band to catastrophic fracture in BMGs. The relationship between the shear-band toughness and the fracture toughness is briefly discussed.

Acknowledgments

The authors are grateful to Dr. H.S. Zhang and Dr. H.L. Li for their assistance in dynamic tests and AFM observations, respectively. Financial support is from the NSFC (Grant Nos. 10725211, 11002144, 11023001 and 11021262), National Natural Science Foundation of China-NSAF (Grant No. 10976100), the National Basic Research Program of China (Grant No. 2009CB724401) and the Key Project of Chinese Academy of Sciences (No. KJCX2-YW-M04). We are very grateful to two anonymous reviewers for their helpful comments, which have improved our manuscript significantly.

References

[1] Schuh CA, Hufnagel TC, Ramamurty U. Acta Mater 2007;55:4067.
[2] Dai LH, Bai YL. Int J Impact Eng 2008;35:704.
[3] Trexler MM, Thadhani NN. Prog Mater Sci 2010;55:759.
[4] Ashby MF, Greer AL. Scripta Mater 2006;54:321.
[5] Wang WH. J Appl Phys 2006;99:093506.
[6] Chen MW. Annu Rev Mater Res 2008;38:14.1.
[7] Schroers J, Johnson WL. Phys Rev Lett 2004;93:255506.
[8] Das J, Tang MB, Kim KB, Theissmann R, Baier F, Wang WH, et al. Phys Rev Lett 2004;94:205501.
[9] Liu YH, Wang G, Wang RJ, Zhao DQ, Pan MX, Wang WH. Science 2007;315:1385.
[10] Conner RD, Li Y, Nix WD, Johnson WL. Acta Mater 2004;52:2429.
[11] Zhang Y, Greer AL. Appl Phys Lett 2006;89:071907.
[12] Jiang MQ, Wang WH, Dai LH. Scripta Mater 2009;60:1004.
[13] Matsumoto R, Miyazaki N. Scripta Mater 2008;59:107.
[14] Conner RD, Johnson WL, Paton NE, Nix WD. J Appl Phys 2003;94:904.
[15] Zhang HW, Maiti S, Subhash G. J Mech Phys Solids 2008;56:2171.
[16] Jiang MQ, Dai LH. Acta Mater 2009;57:2730.
[17] Li J, Spaepen F, Hufnagel TC. Philos Mag 2002;82:2623.
[18] Li QK, Li M. Phys Rev B 2007;75:094101.
[19] Cao AJ, Cheng YQ, Ma E. Acta Mater 2009;57:5146.
[20] Lewandowski JJ, Greer AL. Nat Mater 2006;5:15.
[21] Yang B, Morrison ML, Liaw PK, Buchanan RA, Wang GY, Liu CT, et al. Appl Phys Lett 2005;86:141904.
[22] Neuhäuser H. Scripta Metall 1978;12:471.
[23] Vinogradov AU, Khonik VA. Philos Mag 2004;84:2147.
[24] Liu LF, Dai LH, Bai YL, Wei BC. J Non-Cryst Solids 2005;351:3259.
[25] Jiang WH, Fan GJ, Liu FX, Wang GY, Choo H, Liaw PK. Int J Plast 2008;24:1.
[26] Kim KB, Das J, Lee MH, Yi S, Fleury E, Zhang ZF, et al. J Mater Res 2008;23:6.
[27] Song SX, Nieh TG. Intermetallics 2009;17:762.
[28] Wright WJ, Samale MW, Hufnagel TC, LeBlanc MM, Florando JN. Acta Mater 2009;57:4639.
[29] Klaumünzer D, Maaβ R, Dalla Torre FH, Löffler JF. Appl Phys Lett 2010;96:061901.
[30] Jiang WH, Liu FX, Liaw PK, Choo H. Appl Phys Lett 2007;90:181903.
[31] Jiang MQ, Dai LH. J Mech Phys Solids 2009;57:1267.
[32] Han Z, Wu WF, Li Y, Wei YJ, Gao HJ. Acta Mater 2009;57:1367.
[33] Yang Y, JC YE, Lu J, Liaw PK, Liu CT. Appl Phys Lett 2010;96:011905.
[34] Grady DE. J Mech Phys Solids 1992;40:1197.
[35] Grady DE. Mech Mater 1994;17:289.
[36] Hartman KH, Kunze HD, Meyers LW. In: Meyers MA, Murr LE, editors. Shock waves and high-strain-rate phenomena in metals. New York: Plenum Press; 1981.
[37] Meyers MA, Nesterenko VF, LaSalvia JC, Xue Q. Mater Sci Eng 2001;A317:204.
[38] Kad BK, Gebert J-M, Perez-Prado MT, Kassner ME, Meyers MA. Acta Mater 2006;54:4111.
[39] Pérez-Prado MT, Hines JA, Vecchio KS. Acta Mater 2001;49:2905.
[40] Jiang MQ, Ling Z, Meng JX, Dai LH. Philos Mag 2008;88:407.
[41] Chen H, He Y, Shiflet GJ, Poon SJ. Nature (London) 1994;367:541.
[42] Yang B, Liu CT, Nieh TG, Morrison ML, Liaw PK, Buchanan RA. J Mater Res 2006;21:915.
[43] Guo H, Wen J, Xiao NM, Zhang ZF, Sui ML. J Mater Res 2008;23:2133.
[44] Hampel A, Neuhäuser H. In: Chiem CY, Kunze H-D, Meyer LW, editors. Impact loading and dynamic behaviour of materials, vol. 2. Oberursel: DGM informationsgesellschaft; 1988. p. 845.
[45] Chen HS, Leamy HJ, O'Brien MJ. Scripta Metall 1973;7:415.
[46] Kim J-J, Choi Y, Suresh S, Argon AS. Science 2002;295:654.
[47] Zhang HW, Subhash G, Maiti S. J App Phys 2007;102:043519.
[48] Huang R, Suo Z, Prevost JH, Nix WD. J Mech Phys Solids 2002;50:1011.
[49] Gao YF, Yang B, Nieh TG. Acta Mater 2007;55:2319.
[50] Argon AS. Acta Metall 1979;27:47.
[51] Falk ML, Langer JS. Phys Rev E 1998;57:7192.
[52] Spaepen F. Acta Metall 1977;25:407.
[53] Molinari A. J Mech Phys Solids 1997;45:1551.
[54] Liu LF, Dai LH, Bai YL, Wei BC, Eckert J. J Mater Res 2006;21:153.
[55] Furukawa A, Tanaka H. Nat Mater 2009;8:601.
[56] Grady DE, Kipp ME. J Mech Phys Solids 1987;35:95.
[57] Mott NF. Pros R Soc 1947;A189:300.
[58] Song SX, Nieh TG, Wang XL. Scripta Mater 2010;62:847.
[59] Spaepen F. Nat Mater 2006;5:7.
[60] Johnson WL, Lu J, Demetriou MD. Intermetallics 2002;10:1039.
[61] Heggen M, Spaepen F, Feuerbacher M. J App Phys 2005;97:033506.
[62] Yang Q, Mota A, Ortiz M. Comput Mech 2006;37:194.
[63] Anderson TL. Fracture mechanics. 3rd ed. Boca Raton, FL: Taylor & Francis; 2005. p.34.
[64] Flores KM, Dauskardt RH. J Mech Phys Solids 2006;54:2418.
[65] Xu J, Ramamurty U, Ma E. JOM 2010;62:10.
[66] Jiang MQ, Dai LH. Phys Rev B 2007;76:054204.
[67] Dyre JC. Rev Mod Phys 2006;78:953.

[68] Jiang MQ, Jiang SY, Dai LH. Chin Phys Lett 2009;26:016103.
[69] Lowhaphandu P, Lewandowski JJ. Scripta Mater 1998;38:1811.
[70] Flores KM, Dauskardt RH. Scripta Mater 1999;41:937.
[71] Lewandowski JJ, Wang WH, Greer AL. Phil Mag Lett 2005;85:77.
[72] Raghavan R, Murali P, Ramamurty U. Acta Mater 2009;57:3332.
[73] Escobedo JP, Gupta YM. J App Phys 2010;107:123502.